Global Conformational Changes Control the Reactivity of Methane Monooxygenase†

Stephen C. Gallagher,‡ Anastasia J. Callaghan,§ Jinkui Zhao,|| Howard Dalton,§ and Jill Trewhella*,‡

Chemical Science and Technology Division, Mail Stop G758, Los Alamos National Laboratory, Los Alamos New Mexico 87544, and Biological Sciences, University of Warwick, Coventry, CV47AL, U.K.

Received December 21, 1998; Revised Manuscript Received March 15, 1999

ABSTRACT: We present here X-ray scattering data that yield new structural information on the multicomponent enzyme methane monooxygenase and its components: a hydroxylase dimer, and two copies each of a reductase and regulatory protein B. Upon formation of the enzyme complex, the hydroxylase undergoes a dramatic conformational change that is observed in the scattering data as a fundamental change in shape of the scattering particle such that one dimension is narrowed (by 25% or 24 Å) while the longest dimension increases (by 20% or 25 Å). These changes also are reflected in a 13% increase in radius of gyration upon complex formation. Both the reductase and protein B are required for inducing the conformational change. We have modeled the scattering data for the complex by systematically modifying the crystal structure of the hydroxylase and using ellipsoids to represent the reductase and protein B components. Our model indicates that protein B plays a role in optimizing the interaction between the active centers of the reductase and hydroxylase components, thus, facilitating electron transfer between them. In addition, the model suggests reasons why the hydroxylase exists as a dimer and that a possible role for the outlying γ-subunit may be to stabilize the complex through its interaction with the other components. We further show that proteolysis of protein B to form the inactive B′ results in a conformational change and B′ does not bind to the hydroxylase. The truncation thus could represent a regulatory mechanism for controlling the enzyme activity.

Soluble methane monooxygenase (sMMO) from methanotrophs, such as *Methylococcus capsulatus* (Bath) or *Methylosinus trichosporium* OB3b, catalyzes the biologically and environmentally important conversion of methane to methanol (*1*, *2*). Methane has been implicated as contributing to the greenhouse effect, interacting with atmospheric oxygen to yield CO_2 and water vapor (*3*). sMMO can reduce the amount of methane released to the atmosphere through microbial oxidation. Further, an understanding of the sMMO mechanism of action may help in the design of robust catalysts that can effect the direct oxidation of methane to methanol at ambient temperature and pressure—a reaction that has so far eluded the chemical industry.

The sMMO enzyme has three functional components: the hydroxylase, which is a non-heme diiron-containing protein that exists as a dimer of $\alpha\beta\gamma$-subunits [$(\alpha\beta\gamma)_2$, 250 kDa] and contains the site of oxidation where dioxygen and methane bind; the reductase (38.6 kDa), which contains a 2[Fe−S] cluster and an FAD center and transfers electrons from NAD(P)H to the hydroxylase; and the small (15.8 kDa) regulatory protein B, which has a variety of roles including enhancing electron transfer between the other components, altering the redox potential of the diiron site, changing substrate specificity of the hydroxylase, among others (*2*, *4*−*6*). The regulatory protein B can exist in two forms, one active and an inactive variant (B′) that has lost between 12 and 30 residues from the N-terminus (*5*, *7*, *8*). The evidence for the stoichiometry of the three components in the active sMMO complex (1 hydroxylase dimer:2 reductase:2 protein B) will be discussed below in the context of published data as well as our scattering experiments.

In recent years, there have been great strides toward an understanding of the mode of action of sMMO. In particular, crystallization of the hydroxylase component (*9*, *10*) has allowed a detailed examination of the residues involved in the binding of substrates (*11*) and activation of oxygen required in the oxidation processes (*10*). The field has also benefited from extensive investigation of the mechanism of methane oxidation using kinetic approaches (*12*, *13*). Other techniques, such as EPR, electrochemistry, CD, MCD, EXAFS, and fluorescence spectroscopy (*5*, *14*−*20*), have provided insights into local conformational changes and perturbations which occur upon reduction of the diiron center or binding of the regulatory protein B. To date, however, our knowledge of the physical interactions of the individual components of sMMO has come from interpreting binding studies which give no direct information on global conformational changes that may occur. Small-angle scattering is a powerful technique for probing global conformational changes in proteins arising from the addition of substrates, inhibitors, regulators, and other cofactors (*21*, *22*). In

†This work was performed under the auspices of the Department of Energy under contract to the University of California and was supported by DOE project KP1101010 (J.T.) and the Biotechnology and Biological Sciences Research Council via a studentship (A.J.C.).

* To whom correspondence should be addressed. Phone: 505-667-2031. Fax: 505-667-0100. E-mail: jtrewhella@lanl.gov.

‡ Los Alamos National Laboratory.

§ University of Warwick.

|| Present address: Solid State Division, Oak Ridge National Laboratory, Oak Ridge TN 37831.

10.1021/bi982991n CCC: $18.00
Published on Web 05/06/1999

addition, information on the relative disposition of components within a complex can be obtained. We have therefore used small-angle X-ray scattering to determine the solution conformations of each of the isolated sMMO components and to investigate the effects of binding of the reductase and protein B components on the conformation of the hydroxylase dimer in a single oxidation state. This new structural information helps to explain previous observations about sMMO and also provides new insights into the component interactions, regulatory mechanisms, methane oxidation, and the role of the various protein components in this process.

MATERIALS AND METHODS

Protein Preparation. The hydroxylase and reductase, as well as the B′ form of protein B, were purified from *M. capsulatus* as previously described (*7*). The protein B used in our experiments was a mutant form with a Gln residue substituted for Gly13 in the wild-type sequence, thus making the protein more resistant to inactivation by truncation at this position. This recombinant protein B was expressed in *Escherichia coli* and purified as described previously (*7*). The purified proteins were stored at −70 °C and thawed immediately prior to the scattering experiments. Protein concentrations were initially determined colorimetrically by the method of Bradford (*23*) using bovine serum albumin as a standard and commercially available reagents (Bio-Rad). More accurate protein concentrations were obtained by analysis of the I_0 values from the small-angle scattering data (see below). The sMMO complex was prepared by simple mixing of the components, and its activity was followed by the production of propene oxide in the liquid phase by gas chromatography (*24*) with 25 mM MOPS, pH 7.0, and a preincubation time of 30 s.

X-ray Scattering Data Acquisition and Analysis. X-ray data were collected using either the small-angle X-ray scattering station at Los Alamos described previously (*25*) or our newer instrument which has a two-dimensional detector and a rotating anode source with double focusing mirrors to give a point-source geometry. The data from each instrument gave identical structural parameters for the same protein samples, although the brighter source and two-dimensional detector of the newer instrument give dramatically improved counting statistics. Samples were maintained at 16 °C during data acquisition. Typical data collection times were 10 min to 2 h, depending on protein concentration and molecular mass. All scattering experiments were repeated at least two times using samples from independent preparations.

Scattering data were reduced and analyzed as previosuly described (*25*). Parameters used in the interpretation of the scattering data included radius of gyration, R_g, forward (or zero-angle) scattering intensity, I_0, and the pairwise length distribution function, $P(r)$. $P(r)$ is the probable frequency of vector lengths connecting small-volume elements within the scattering particle. $P(r)$, therefore, goes to zero at the maximum linear dimension of the particle, d_{max}. For a dilute solution of monodisperse, identical particles the scattering intensity, $I(Q)$, and $P(r)$ are related by a Fourier transformation:

$$P(r) = r^2/2\pi^2 \int I(Q)Q^2(\sin(Qr)/Qr)\, dQ \qquad (1)$$

where $Q = (4\pi \sin\theta)/\lambda$ is the amplitude of the scattering vector, θ is half the scattering angle, and λ the wavelength of the scattered radiation (1.54 Å). $P(r)$ is calculated from the experimental scattering profile using an indirect Fourier transform method (*26*). R_g and I_0 are calculated as the second and zeroth moments of $P(r)$, respectively.

I_0, when normalized to molar concentration, is proportional to the square of the molecular weight for particles with the same mean scattering densities. By using a standard protein of known molecular weight (lysozyme in this study), one can determine the molecular weight of another monodisperse protein sample by taking ratios of the I_0 values. An I_0 analysis can thus be use to check the monodispersity in samples of known protein concentration or to determine accurate protein concentrations for solutions known to be monodisperse (*27*). In addition, I_0 is highly sensitive to complex formation (*27*). For a three component system with component molecular weights M_a, M_b, and M_c, I_0 is proportional to $(M_a + M_b + M_c)^2$ for the 1:1:1 complex but to the much smaller $M_a^2 + M_b^2 + M_c^2$ if the components do not form a complex. For a mixture of partially complexed components, I_0 is proportional to the concentration-weighted average of the I_0 values for the complexed and uncomplexed components.

Molecular volumes were calculated from the scattering data using the equation:

$$V = 2\pi^2 I_0/Q_i \qquad (2)$$

where Q_i is the scattering invariant (*28*):

$$Q_i = \int Q^2\, dQI(Q) \qquad (3)$$

Because the scattering data are measured only over a finite Q-range, the scattering invariant, and hence molecular volume, calculations are subject to systematic error. These errors vary for different experiments and in our case are of the order of 10% based on comparison of the expected volumes with those calculated from the scattering data.

Modeling the Scattering Data. In the absence of high-resolution crystal structure data, the scattering from globular proteins can be effectively modeled using uniform-density ellipsoid shapes (*29*, *30*). Protein B and the reductase were each modeled as uniform density ellipsoids, and model scattering profiles were calculated using a Monte Carlo simulation program [SASMODEL (*30*)]. SASMODEL generates models using one or more ellipsoid shapes with dimensions constrained within a range given by the user. Large numbers of models are generated by an algorithm that assigns random values (within the defined constraints) to the lengths of each semi-axis. For each model generated, a $P(r)$ function is calculated using a rapid Monte Carlo integration method (*25*) in which the ellipsoids are filled with random points and all possible vector lengths between the points are summed to give $P(r)$. Model $P(r)$ functions based on the hydroxylase crystal structure [Protein Data Bank (PDB) accession no. P22869], as well as for the sMMO complex, were calculated using a program (PRPDB) that utilizes a rapid Monte Carlo integration method similar to that used by SASMODEL. The atomic coordinates from the crystal structure are placed in a box with a three-dimensional grid. An option to include a hydration layer, in which the solvent layer at the surface of the protein is assigned a different mean scattering density to the bulk solvent, is included. The

thickness and contrast of the hydration layer are parameters that can be chosen by the user. The volume elements of the grid are assigned scattering density values based on the number of electrons that fall within the volume element (from either the protein or hydration layer components). Alternatively, a uniform density can be assigned to grid elements occupied by the structure. The model $P(r)$ is calculated by filling each volume element occupied by the molecular shape with 4000 random points and summing all vector-lengths between pairwise combinations of the saved points. PRPDB can also use the output from SASMODEL and calculate $P(r)$ profiles from uniform density ellipsoid shapes as well as composite models made up from uniform density ellipsoids combined with crystal structure coordinates. Typically, 4000 points were used in our model $P(r)$ calculations which gave smooth well-determined profiles. Both SASMODEL and PRPDB calculate model scattering profiles for comparison with experiment by Fourier transformation of $P(r)$. Model fits are evaluated using least-squares methods and saved in PDB format for ease of viewing.

RESULTS AND DISCUSSION

Analysis of the sMMO Component Structures. To evaluate the sMMO component structures, as well as to aid in interpretation of the scattering profile of the sMMO complex, we first measured the solution-scattering profiles of each of the isolated components (Figure 1). Scattering data were measured for a series of five protein concentrations in the range 2−15 mg/mL, in 25 mM MOPS, pH 7.0, $T = 13$ °C. For each component, there was no concentration dependence of the scattering data, indicating that interparticle interference effects (*31*) were negligible and hence required no correction. The vector length distribution functions for each component, calculated as the inverse Fourier transform of the scattering profiles (*26*), are shown in Figure 2. The best-fit ellipsoid models for the reductase and protein B have approximate dimensions 72, 44, 32 Å and 50, 34, 30 Å, respectively. These models give reduced χ^2 values of 1.03 and 1.01, respectively, indicating a near perfect fit (which would have $\chi^2 = 1.0$) to the scattering data. For the isolated hydroxylase, a model $P(r)$ function was calculated using the crystal structure coordinates (*10*). This fit gives $\chi^2 = 0.99$ without inclusion of a hydration layer. Thus, under the conditions of our experiments, hydration layer effects are not detected and the crystal and solution structures for the hydroxylase are the same. Figures 1 and 2 show the excellent fits of the model $I(Q)$ and $P(r)$ functions to those derived from experiment for each component.

The reductase and protein B components give unimodal $P(r)$ profiles typical for compact globular proteins (Figure 2a). In contrast, the $P(r)$ function for the hydroxylase is bimodal with a shoulder at 70 Å (Figure 2b). This shoulder is due to the bilobal shape of the hydroxylase that arises from the way in which the two $\alpha\beta\gamma$ trimers associate to form the dimer (Figure 3). The values obtained for d_{max}, R_g, and molecular volume for each of the isolated components are in good agreement with the expected values based on monodisperse proteins of mass 250, 38.6, and 15.8 kDa, for the hydroxylase, reductase, and protein B, respectively, and assuming a specific volume of 0.74 cm^3/g (Table 1). The molecular volumes were calculated from the scattering data using eqs 2 and 3 (Materials and Methods).

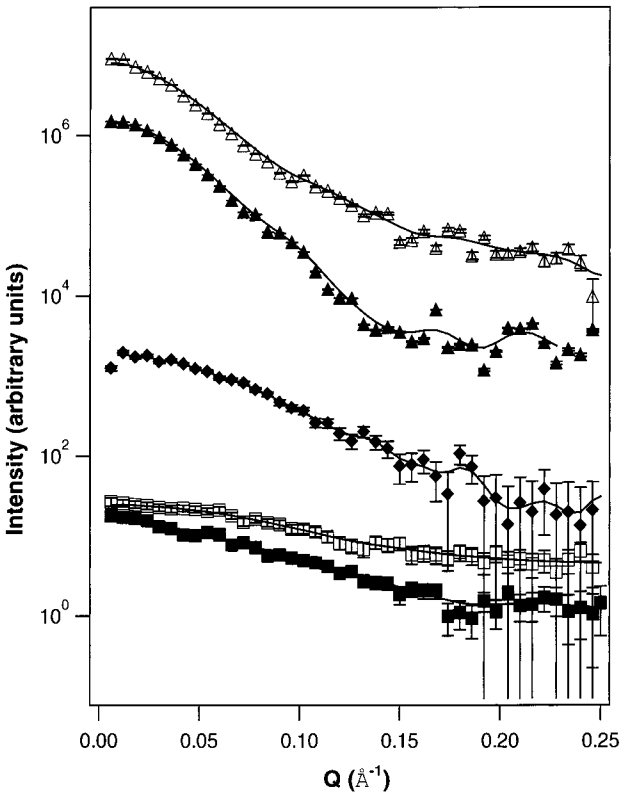

FIGURE 1: $I(Q)$ versus Q data for sMMO and its individual components. Experimental data are depicted by the symbols; protein B (■), B′ (□), reductase (◆), hydroxylase (▲), sMMO (1:10:10 mixture = 1:2:2 complex) (△). The scattering profiles are offset by multiplication factors in order to separate them on the vertical axis for easy viewing (0.2, 4, 16, 258, and 4096, respectively). The errors indicated are based on counting statistics only. The solid lines represent the model $I(Q)$ profiles calculated using uniform ellipsoids for the reductase, protein B and B′, and the crystal structure coordinates for the hydroxylase. For the sMMO complex, the solid line represents the model profile calculated using the model shown in Figure 6.

Structural Differences between Protein B and B′. Figure 2a shows a comparison of the $P(r)$ functions for protein B and B′. A significant increase in d_{max} is observed for B′ compared with B. The best-fit ellipsoid which approximated the scattering from B′ has dimensions 66, 28, and 27 Å ($\chi^2 = 1.02$) compared to 50, 34, and 30 Å for protein B, i.e., B′ is longer and thinner than B. (As a measure of the discrimination between these fits to the data one can compare the scattering data for B to the best-fit ellispoid determined for B′ which gives a χ^2 of 12.5. Vice versa, the experimental data for B′ compared to the best-fit model for B gives a χ^2 of 13.0). The measured I_0 values and molecular volumes show that both protein B and B′ are monodisperse in solution, indicating that the observed changes in structural parameters cannot be attributed to aggregation (Table 1). The observed extension of the structure upon removal of the N-terminal segment of protein B therefore must be due to a partial unfolding or to some sort of opening of the structure triggered by the loss of interactions with the N-terminal residues. In subsequent scattering experiments on mixtures of the hydroxylase with the reductase plus protein B or B′ under conditions whereby binding of B is observed (see below),

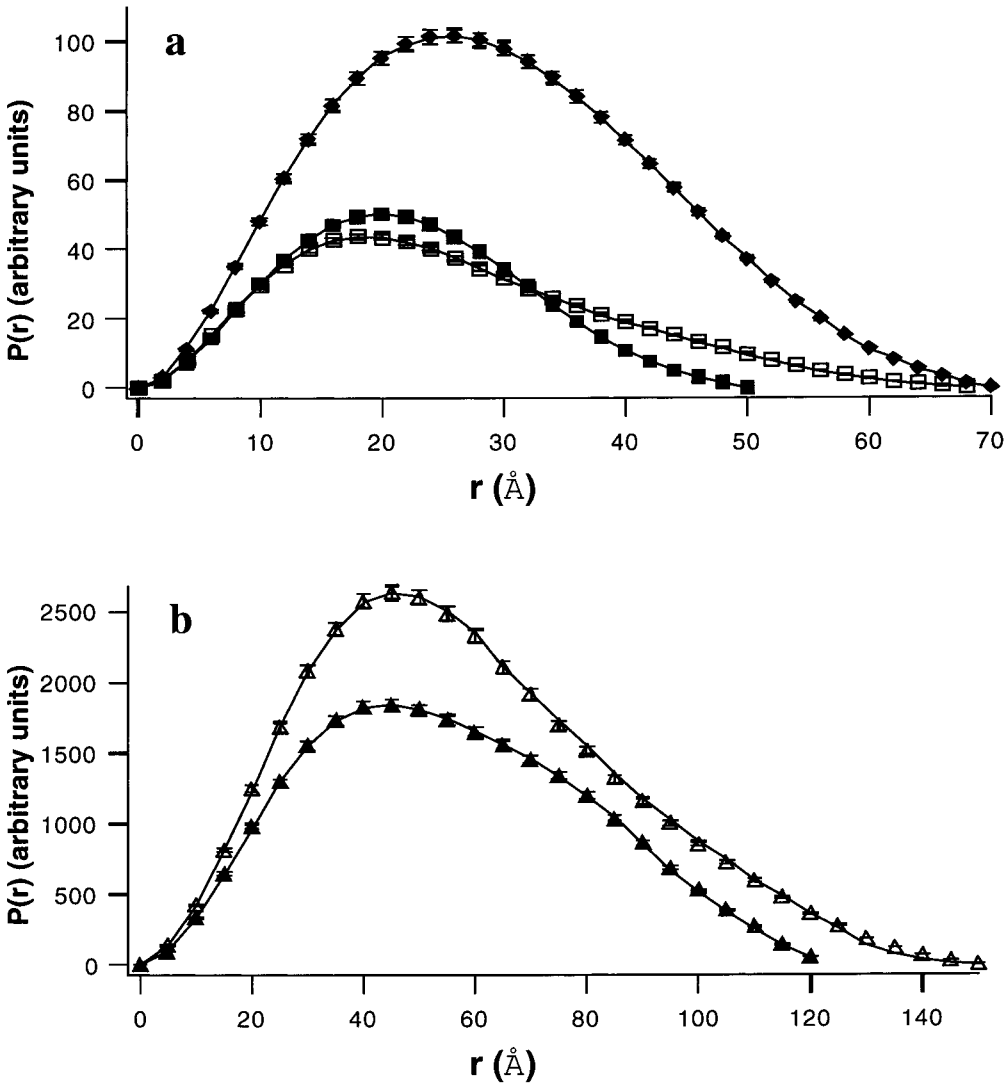

FIGURE 2: $P(r)$ functions for sMMO and its individual components. The experimentally derived $P(r)$ functions for (a) protein B (■), B′ (□), reductase (◆), and (b) hydroxylase (▲), sMMO (1:10:10 mixture = 1:2:2 complex) (△). The solid lines are the $P(r)$ functions calculated for the models indicated in Figure 1. The $P(r)$ profiles are scaled such that their areas are proportional to the molecular weight of the component or complex for convenient comparison of shape changes.

there is no evidence for binding of B′, including in the I_0 data that are most sensitive to complex formation.

Several authors have suggested that the in vivo proteolytic cleavage of the 12 N-terminal residues of protein B to yield an inactive form of the protein, designated as B′, may represent a means for controlling activity of the enzyme complex (*5*, *7*, *8*). In the absence of methane, the uncoupling of sMMO activity from NADH oxidation by inactivation of protein B would prevent consumption of limited cellular NADH resources. Kazlauskaite and coauthors (*5*), for example, found that although protein B alters the potentials at which the hydroxylase component is reduced, B′ does not. It has been unclear, however, how the loss of the 12 N-terminal residues of protein B (to give B′) results in inactivation. The scattering data show that a conformational change occurs in B upon cleavage of the N-terminal segment and binding is inhibited.

Titration of Hydroxylase with Reductase Plus Protein B to Determine Stoichiometry within the sMMO Complex. Scattering data were measured from mixtures of the sMMO components with 1:1:1, 1:2:2, 1:5:5, 1:10:10, and 1:20:20 ratios of hydroxylase:reductase:protein B. The measured I_0 value is proportional to the square of the molecular weight of the scattering particle and, for protein solutions of known concentration, is extremely sensitive to molecular associations (see Materials and Methods). Analysis of the I_0 values indicate that 0, ≤10, and ≤25% of the total protein B and reductase were bound to the hydroxylase for the 1:1:1, 1:2:2, and 1:5:5 mixtures, respectively (Table 1). This minimal binding is consistent with the minimal changes observed in R_g and $P(r)$ compared to the isolated hydroxylase. The I_0 values for the 1:10:10 and 1:20:20 mixtures are consistent with formation of the 1:2:2 complex with 8 and 18 free equiv of the reductase and protein B, respectively. Figure 4 shows a plot of the observed I_0 values for the mixtures plotted against the molar ratio of (reductase and protein B) to hydroxylase in the solution. Also shown are the expected I_0 dependencies assuming different stoichiometries of hydroxylase:reductase:protein B. The comparisons show clearly that the observed data fit the 1:2:2 complex being formed with ≥10 equiv of protein B and reductase compared to the hydroxylase. The discrimination between the different stoichiometries is excellent and well beyond the errors in the data.

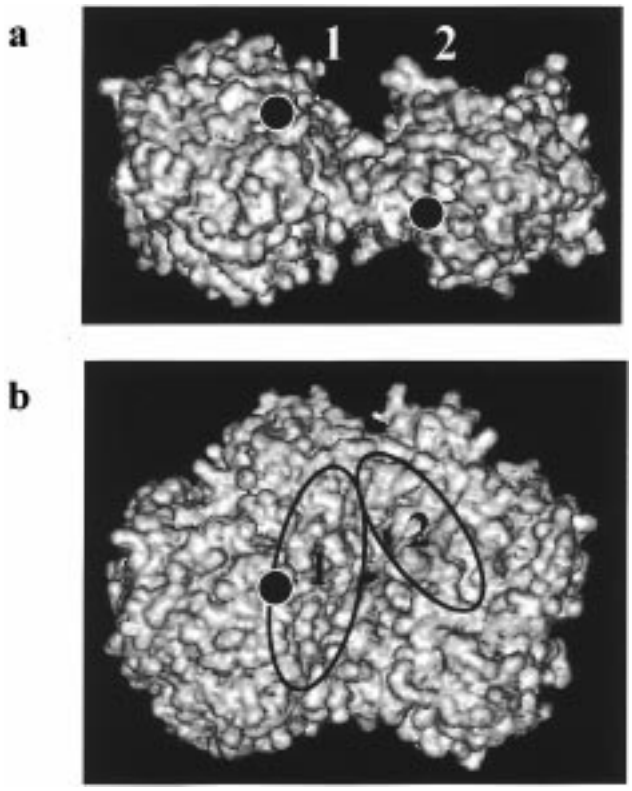

FIGURE 3: Hydroxylase crystal structure. (a) Surface representation showing the bilobal nature of the dimerized trimers (*11*). The active sites are indicated (●). The structure has been rotated to show the two canyon-like features (1 and 2) which previously had been proposed as possible binding sites of protein B and the reductase (*9*). (b) Top view of the structure in panel a showing the positions of the two canyons.

The scattering results are consistent with prior evidence for the physical interactions within the sMMO complex, including titrations of the hydroxylase with reductase and protein B, which give an optimum ratio for activity at 1:2:2 (hydroxylase: reductase: protein B) (*15*); cross-linking studies which provided a tentative assignment of the binding sites of protein B and reductase to the hydroxylase (*20*); the crystal structure of the hydroxylase in the presence of a short peptide of the reductase component (*32*); and perturbation of the partially and fully reduced EPR signal of the hydroxylase by addition of protein B (*20*). Combined, these data suggest possible sites of interaction between the three components and that the stoichiometry of components within the complex is 1:2:2. The stoichiometry of components within the sMMO complex has also be implied from the dimeric form of the hydroxylase, which suggests that two equivalents of the reductase and protein B will be required to bind to a single hydroxylase dimer (*9*).

Because interpretation of small-angle scattering data in structural terms requires a homogeneous solution of monodisperse, identical particles, our titration experiments were done in the absence of NAD(P)H and substrates in order to prevent turnover which would result in a mixture of different states. Under these conditions, 10 equiv each of the reductase and protein B are required to see full complex formation, whereas maximal activity of sMMO from *Methylosinus thrichosporium* OB3b is observed for mixtures containing 2 equiv of both the reductase and protein B per hydroxylase (*15*). It therefore appears that the addition of NAD(P)H and/or substrate may increase the affinity of the reductase and protein B to the hydroxylase, thus driving the equilibrium toward complex formation.

Structural Changes Observed Upon Binding of Reductase and Protein B to the Hydroxylase. To determine the structural parameters of the sMMO complex, we used the scattering data from the 1:10:10 mixture of hydroxylase:reductase: protein B. The 8 free equiv of reductase and protein B in this mixture make relatively small contributions to the scattering (4% and 10% total intensity for protein B and reductase, respectively) due to their small size compared to the complex. This contribution is most evident in the overall intensity and I_0 values, and will be less evident in the shape of the scattering profile from which the particle shape parameters are calculated. Since we know the amount of free protein B and reductase, as well as their scattering profiles, we can subtract their contributions proportionately according to their known concentrations. These corrected curves gave $P(r)$ profiles, R_g and d_{max} values that are indistinguishable, within the limits of the experimental errors, from those calculated from the uncorrected data. Nevertheless, all of the interpretation and modeling for the sMMO complex were done using these corrected data.

Accompanying formation of the 1:2:2 sMMO complex, we observe in the $P(r)$ profiles an increase in d_{max}, from 125 to 150 Å and the shoulder at 70 Å is lost, indicating that its overall structure is more elongated and has lost the bilobal character of the hydroxylase alone (Figure 2b). In addition, the R_g value for the scattering particle increases from 42 to 46 Å and the molecular volume increases by 26%. This latter increase is, within the statistical error, what is expected for the formation of a 1:2:2 complex (Table 1).

The single ellipsoid fit to the scattering data for the complex gives dimensions 150, 71, and 66 Å with a χ^2 value of 1.04. In comparison, the best-fit ellipsoid for the isolated hydroxylase calculated from the crystal structure coordinates has dimensions of 125, 95, and 65 Å, which agree well with those of the best-fit ellipsoid calculated from the scattering data 127, 98, and 65 Å ($\chi^2 = 1.01$). These ellipsoid fits indicate that the molecular envelopes of both the hydroxylase and the complex can be reasonably approximated with uniform density ellipsoid models. Importantly, upon complex formation and the accompanying increase in d_{max}, there is a narrowing in a second dimension (by 24 Å, or 25%), indicating that the hydroxylase cannot be accommodated within the molecular envelope of the complex without a conformational change. The point is illustrated in Figure 5 which shows the best fit ellipsoids for the hydroxylase and the sMMO complex superimposed with the crystal structure for the hydroxylase and the hydroxylase in the sMMO complex derived from the scattering data (see below).

Parallel scattering experiments in which the hydroxylase was titrated either with the reductase or protein B alone, up to 10 equiv of each, showed no evidence for their binding to the hydroxylase, either in terms of the expected increases in I_0 values or conformational changes. These results show that both the reductase and protein B are required for binding and inducing the conformational change

Modeling the sMMO Complex. The crystal structure of the hydroxylase shows two extended canyon-like features

Table 1: R_g, d_{max}, and Molecular Volumes for Each Component of sMMO and Component Mixtures[a]

component/mixture	R_g (Å)	d_{max} (Å)	measured I_0 (arbitrary units)	measured volume (Å^3)	expected volume (Å^3)
protein B	17.5 ± 0.9	50	3950 ± 150	19 200 ± 3100	19 400
protein B'	19.8 ± 0.9	70	3650 ± 160	20 300 ± 1700	17 900
reductase	23.1 ± 0.4	70	9650 ± 470	43 200 ± 2000	47 300
hydroxylase	41.1 ± 0.04	125	62 500 ± 2100	275 000 ± 1800	305 800
1:1:1	42.1 ± 0.7	125	67 350 ± 2200	298 100 ± 13 100	
1:2:2	43.3 ± 1.6	125	71 020 ± 2350	280 700 ± 29 200	
1:5:5	44.1 ± 0.6	130	121 520 ± 3520	294 600 ± 19 200	
1:10:10	46.4 ± 0.4	150	185 000 ± 2680	346 300 ± 11 800	
1:20:20	46.5 ± 0.5	150	264 200 ± 2450	348 200 ± 10 040	

[a] Errors indicated are based on counting statistics alone. Expected volumes are calculated using eqs 2 and 3 in Materials and Methods and a partial specific volume of 0.74 cm^3/mg (*37*). The expected volume for a 1:2:2 complex of the hydroxylase:reductase:protein B is 373 900 Å^3. In absolute terms, the volumes determined from the scattering for the hydroxylase and the complex are ~90% of the values expected based on calculation from their specific volumes and molecular mass, with ~4% statistical error. This agreement is excellent given the finite Q-range of the experimental data (see Materials and Methods).

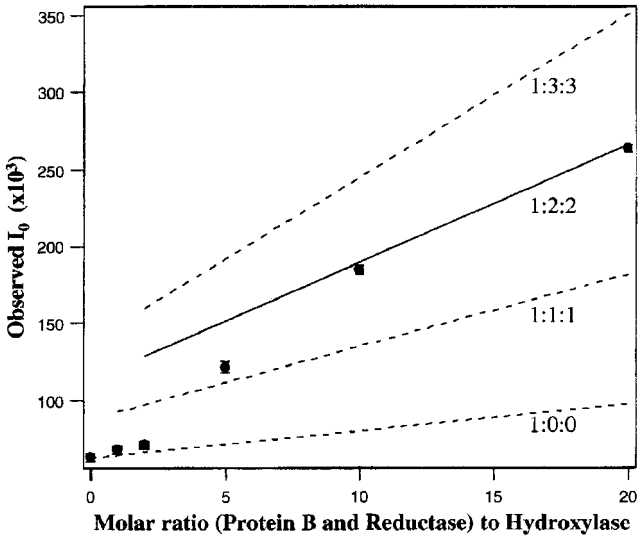

FIGURE 4: Titration of the hydroxylase with protein B and reductase. The I_0 values measured for the mixtures of hydroxylase: reductase:protein B plotted as a function of the protein B and reductase to hydroxylase mole ratio. The solid line indicates the expected I_0 values assuming two equivalents of protein B and reductase bind to one hydroxylase. The dashed lines correspond to alternative stoichiometries for binding as indicated.

(Figure 3) which have been proposed as potential binding sites for the reductase and protein B (*9*). Models for the complex in which protein B and the reductase were positioned so that they filled these canyon-like features, however, cannot account for the increases in R_g and d_{max} observed upon complex formation. The best χ^2 obtained for such models compared with the scattering data was 16.0, a result that is not surprising since we know that the overall dimensions of the hydroxylase cannot fit within the molecular envelope calculated for the complex. It is possible to obtain the observed increase in the d_{max} for the complex by positioning protein B or the reductase on the surface of the hydroxylase in highly extended arrangements. These types of models, however, do not give the correct R_g values or shape functions. In general, they do not have the correct ratios of d_{max} to cross-sectional area for the elongated shape of the complex, and models of this type all gave χ^2 values ≥ 6, indicating poor fits.

Inspection of the hydroxylase structure suggests that the required conformational change can be achieved via a rearrangement of the two trimers that associate to form the hydroxylase dimer. Within each trimer, the individual subunits have convoluted surfaces of interaction, whereas the two trimers contact each other with relatively small areas of interaction at each end of their long axes between the two β-subunits. At one end of this interaction, there is a planar interface of approximately 200 Å^2. This planar interface provides a potential pivot point in the structure about which the hydroxylase can rotate to give a structure with an increased d_{max}, while maintaining a significant area of contact between the trimers. Rotating about this pivot point takes advantage of the long axes of the trimers to obtain the increase in d_{max} of 25 Å while at the same time narrowing the structure in a second dimension (Figure 5). To test this hypothesis against the scattering data, the hydroxylase was rotated systematically in 10° steps, about the pivot point so as to increasingly extend the long axis of the hydroxylase dimer interface. At the same time, best-fit ellipsoid models of the reductase and protein B (two of each) were placed as close to the hydroxylase active site such that they sat within the overall ellipsoid dimensions for the complex. Model $P(r)$ functions were determined and compared to the experimental $P(r)$ function. If the extension of the hydroxylase structure in this manner accounts predominantly for the increase in d_{max}, one hydroxylase trimer would have to rotate approximately 180° with respect to the second to fit the scattering data (Figures 5 and 6). This rotation preserves the 2-fold symmetry expected for the dimer. It also increases the distance between the active sites from 45 to 75 Å. A plot of log $I(Q)$ vs Q for the experimental data from the complex and that determined from the model (Figure 1) shows the quality of this model fit to the data ($\chi^2 = 1.13$). Further, the model $P(r)$ agrees well with that determined from the experimental data (Figure 2b). There is likewise excellent agreement for the structural parameters determined for the model and the experimental data. Both have a d_{max} of 150 Å, the R_g values are both 46 Å and the volumes agree within 10% (346 300 Å^3 for the experimental and 379 100 Å^3 for the model).

Interpretation of the sMMO Model and Relationship to Previous Work. The precise binding site of the reductase and protein B components on the extended form of the hydroxylase cannot be determined from the X-ray scattering data alone. Further, we cannot rule out the possibility of there being some small rearrangements of the subunits within the hydroxylase trimers as the dimer opens. However, Figure 6 shows our model for the interaction between the extended hydroxylase and the other components that gives the best

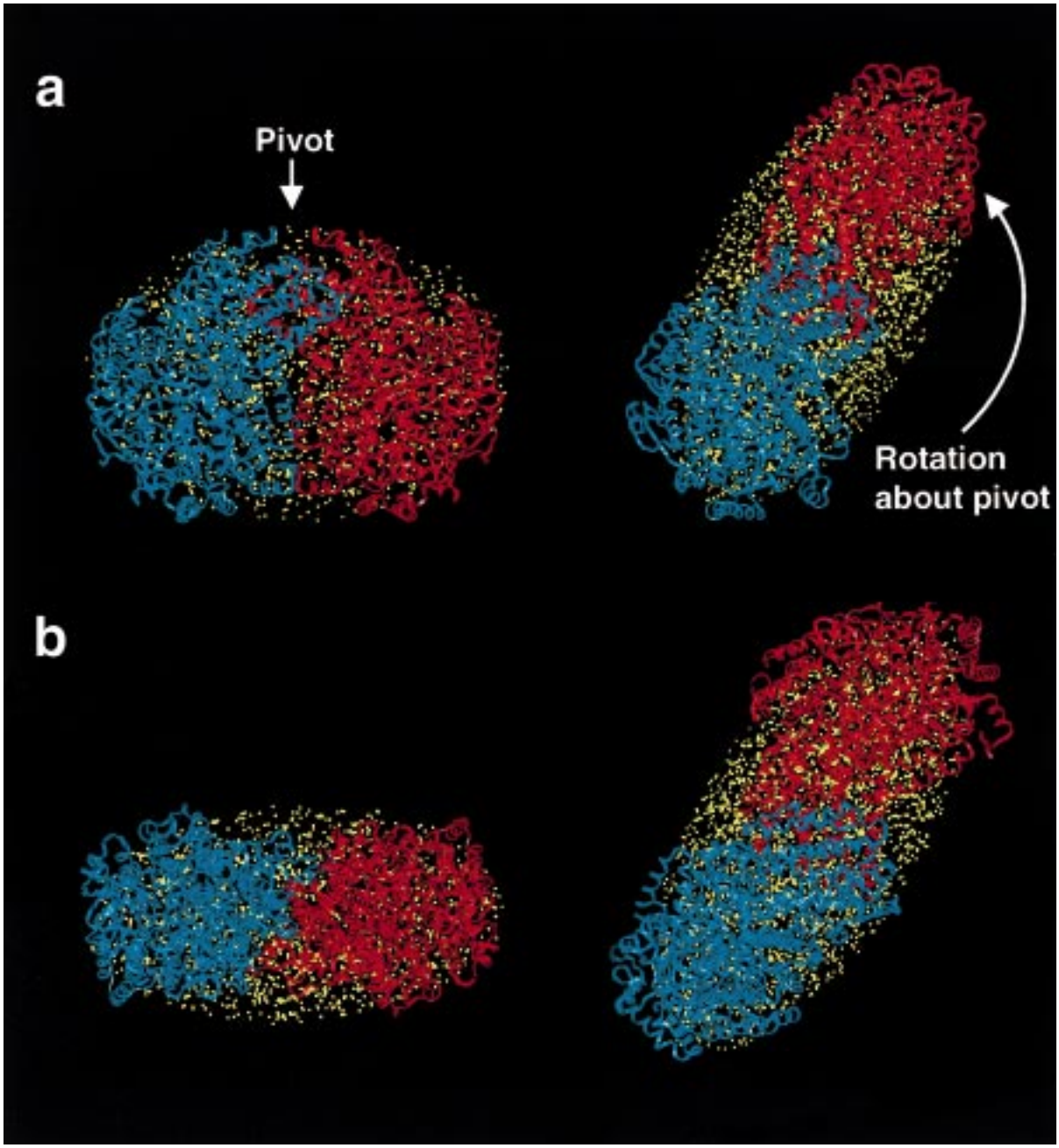

FIGURE 5: Proposed model for the extended hydroxylase structure. Ellipsoid models for the isolated hydroxylase dimer (left) and the sMMO complex (right) are shown as yellow dots that fill the ellipsoid volumes. The upper and lower representations (a and b) are obtained by rotating the respective structures 90° about their long axes. A ribbon representation of the hydroxylase structure is superimposed on the ellipsoids, with the individual trimers that associate to form the dimer colored blue and red. The two orientations of the isolated hydroxylase are shown (left) with the ribbon representations based on the unmodified crystal structure. For the complex (right), the hydoxylase dimer is shown in an extended configuration obtained by a rotation of the long axes of each trimer about a pivot plane between the trimers, opening them by approximately 180°. Note, the orientation of the blue trimer is held constant in the views shown in panel a to aid in the comparison. The reorientation of the hydroxylase dimer upon forming the complex accounts for the observed increase in d_{max} as well as the narrowing of the structure in a second dimension. The bound protein B and reductase (shown in Figure 6) fit within the unfilled portion of the ellipsoid for the complex.

fit to our scattering data consistent with everything we currently know about sMMO. In this model, protein B binds close to the pivot point in the hydroxylase, and we propose that it plays a role in maintaining the extended form of the hydroxylase dimer. This arrangement would allow the reductase component to bind close to the hydroxylase active site and could, therefore, represent the manner in which protein B enhances electron transfer, binding of molecular oxygen, and substrate oxidation (*5*). No evidence for complex formation, or conformational changes, was observed upon addition of either the reductase or protein B alone to the hydroxylase, indicating that both are required to bring about the conformational change under the equilibrium conditions of the scattering experiments. It appears then that protein B may facilitate the conformational change of the hydroxylase, but that the reductase is also required and may play a role in locking the hydroxylase in the extended configuration. Hydrogen peroxide can provide electrons and oxygen to the hydroxylase for the methane oxidation reaction in the absence of the reductase and protein

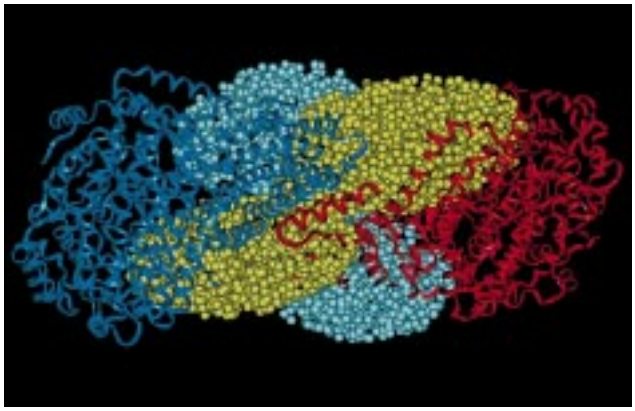

FIGURE 6: Model of the interaction between the three components of sMMO. The hydroxylase structure is shown in ribbon form (dark blue and red), protein B (light blue), and the reductase (yellow) are represented by ellipsoids filled with small spheres. The rotation of the hydroxylase trimers about the pivot region shown in Figure 5 allows B and C to bind closely the hydroxylase giving a compact structure with protein B and the reductase interacting with the active sites. The ellipsoids of the reductase and protein B are effectively rotational averages of their structures. As a result, their volumes are somewhat larger than the actual protein structure is (51 600 and 26 700 Å^3 for the ellipsoid models compared to 43 300 and 19 200 Å^3 for the reductase and protein B, respectively), and they therefore were allowed to overlap some with the hydroxylase such that they fit within the overall molecular boundary for the complex.

B (*33*). Addition of hydrogen peroxide up to concentrations of 100 mM did not give rise to any conformational change in the hydroxylase as evidenced by the scattering data. This result supports our proposal that the role of protein B is primarily to facilitate the conformational change in the hydroxylase in order to allow close interaction between the reductase and hydroxylase. Our model for the complex also suggests why the hydroxylase exists as a dimer since contacts between protein B and both of the hydroxylase trimers occur. These contacts could enhance the interactions between the reductase and protein B with the hydroxylase.

We have compared the interactions between the components in our model with other data collected under equilibrium conditions such as chemical cross-linking studies (*20*) and the crystal structure of the hydroxylase in association with a short peptide from the reductase (*32*). The primary interactions suggested from these data are between the reductase and the α- and β-subunits (crystal and cross-linking data) and between protein B and the α-subunit (cross-linking studies only). Our model supports these assignments, but also suggests that there are further interactions. Indeed there appear to be interactions between the reductase and protein B with all three subunits of the hydroxylase. The active site is centered in the α-subunits, and the surface of interaction between the two hydroxylase trimers is provided by the β-subunit. The γ-subunit, however, is situated toward the outside of the hydroxylase dimer, and its precise role has been to date unclear. The scattering data presented here suggest that the γ-subunit contributes to the overall stability of the complex by providing additional interactions with protein B.

Our scattering data on the fully oxidized hydroxylase are also consistent with previous electrochemical and EPR experiments carried out under nonequilibrium conditions during reduction of the hydroxylase. The electrochemical measurements suggest that while protein B can alter the reduction potentials of the hydroxylase in the absence of reductase, B′ cannot (*5*). In addition, Fox and co-workers (*20*) showed that the EPR spectrum of the hydroxylase is altered by addition of protein B. If the binding of protein B were to affect the hydroxylase in the manner proposed here, it would most certainly affect the environment of the diiron center thus explaining the alteration in its EPR spectrum and redox potentials (*5*, *20*). In addition to the effects on the environment of the diiron center of the hydroxylase, the proposed close association between protein B and the hydroxylase suggests how protein B could alter the hydroxylase substrate specificity (*15*). Protein B is positioned such that it can be involved in recognition of substrates entering the hydroxylase active site. A similar proposal was suggested for phenol hydroxylase, a closely related enzyme (*34*).

CONCLUSIONS

In summary, we have shown that formation of the sMMO complex results in a conformational change in the hydroxylase that involves an extension in one dimension and a narrowing in a second. We have proposed a model that fits the scattering data for the complex in which the pair of trimers that associate to form the hydroxylase dimer are rotated with respect to each other about a pivot plane such that the 2-fold symmetry expected for a dimer is preserved. The best-fit model of the complex is a compact structure containing one hydroxylase dimer and two molecules each of the reductase and protein B, and requires close interaction between all of the protein components. In the model, the conformational change in the hydroxylase allows the reductase to bind close to the hydroxylase active site. Both protein B and the reductase are required for the conformational change. The reductase thus not only provides reducing power for the methane oxidation process but also appears to act in concert with protein B to induce the extended conformation of the hydroxylase dimer. Inactivation of protein B to B′ by cleavage of 12 N-terminal residues is accompanied by a conformational change that renders the protein unable to bind and alter the global structure of the hydroxylase. This inhibition of binding provides a means to regulate the activity of the enzyme in vivo.

There are other examples of regulation of enzyme activity via conformational changes induced by proteins binding and modulating access to, or the configuration, of the active site. An example is the binding of calmodulin to the autoinhibitory region of myosin light chain kinase that results in its removal from the surface of the catalytic core and a subsequent closure of the catalytic cleft upon substrate binding (*35*, *36*). The sMMO example presented here involves a much more dramatic movement of molecular mass, however, than the more typical calmodulin/kinase/substrate interaction and associated conformational transitions.

ACKNOWLEDGMENT

We thank Dominico Vigil for technical assistance with the X-ray data collection and Brian MacDonald for technical assistance with the X-ray instrumentation. We thank Susan Slade for her help in the preparation of proteins.

REFERENCES

1. Liu, K. E., and Lippard, S. J. (1995) *Adv. Inorg. Chem. 42*, 263.

2. Colby, J., and Dalton, H. (1978) *Biochem. J. 171*, 461.
3. Badr, O., Probert, S. D., and Ocallaghan, P. W. (1992) *Appl. Energy 41*, 95.
4. Fox, G. G., Froland, W. A., Dege, J. E., and Lipscomb, J. D. (1989) *J. Biol. Chem. 264*, 10023.
5. Kazlauskaite, H., Hill, A., Wilkins, P. C., and Dalton, H. (1996) *Eur. J. Biochem. 241*, 552.
6. Liu, Y., Nesheim, J. C., Lee, S.-K., and Lipscomb, J. D. (1995) *J. Biol. Chem. 270*, 24662.
7. Lloyd, J. S., Bhambra, A., Murrell, J. C., and Dalton, H. (1997) *Eur. J. Biochem. 248*, 72.
8. Shinohara, Y., Uchiyama, H., Yagi. O., and Kusakabe, I. (1998) *J. Ferment. Bioeng. 85*, 37.
9. Rosenzweig, A. C., Frederick, C. A., Lippard, S. J., and Nordlund, P. (1993) *Nature 366*, 537.
10. Rosenzweig, A. C., Nordlund, P., Takahara, P. M., Frederick, C. A., and Lippard, S. J. (1995) *Chem. Biol. 2*, 409.
11. George, A. R., Wilkins, P. C., and Dalton, H. (1996) *J. Mol. Catal. 2*, 103.
12. Liu, K. E., Valentine, A. M., Wang, D., Huynh, B. H., Edmunson, D. E., Salifgou, A., and Lippard, S. J. (1995) *J. Am. Chem. Soc. 117*, 10174.
13. Nesheim, J. C., and Lipscomb, J. D. (1996) *Biochemistry 35*, 10240.
14. Woodland, M. P., Patil, D. S., Cammack, R., and Dalton, H. (1986) *Biochim. Biophys. Acta 873*, 237.
15. Froland, W., Andersson, K. K., Lee, S. K., Liu, Y., and Lipscomb, J. D. (1992) *J. Biol. Chem. 267*, 17588.
16. Rosenzweig, A. C., and Lippard, S. J. (1994) *Acc. Chem. Res. 27*, 229.
17. Paulsen, K. E., Liu, Y., Fox, B. G., Lipscomb, J. D., Munck, E., and Stankovich, M. T. (1994) *Biochemistry 33*, 713.
18. Davydov, A., Davydov, R., Graslund, A., Lipscomb, J. D., and Andersson, K. K. (1997) *J. Biol. Chem. 272*, 7022.
19. C−Pulver, S., Froland, W. A., Lipscomb, J. D., and Solomon, E. I. (1997) *J. Am. Chem. Soc. 119*, 387.
20. Fox, B. G., Liu, Y., Dege, J. E., and Lipscomb, J. D. (1991) *J. Biol. Chem. 266*, 540.
21. Trewhella, J. (1997) *Curr. Opin. Struct. Biol. 7*, 702.
22. Trewhella, J., Gallagher, S. C., Krueger, J., and Zhao, J. (1998) *Sci. Prog. 81*, 101.
23. Bradford, M. (1976) *Anal. Biochem. 72*, 248.
24. Pilkington, S., Salmond, G., Murrell, J. C., and Dalton, H. (1990) *FEMS Microbiol. Lett. 72*, 345.
25. Heidorn, D. B., and Trewhella, J. (1988) *Biochemistry 27*, 909.
26. Moore, P. B. (1980) *J. Appl. Crystallogr. 13*, 168.
27. Krueger, J. K., Bishop, N. A., Blumenthal, D. K., Zhi, G., Beckingham, K., Stull, J. T., and Trewhella, J. (1998) *Biochemistry 37*, 17810.
28. Porod, G. (1982) in *Small-Angle X-ray Scattering* (Glatter, O., and Kratky, O., Eds.) Academic Press, London.
29. Henderson, S. J., Newsholme, P., Heidorn, D. B., Mitchell, R., Seeger, P. A., Walsh, D. A., and Trewhella, J. (1992) *Biochemistry 31*, 437.
30. Zhao, J., Hoye, E., Boylan, S., Walsh, D. A., and Trewhella, J. (1998) *J. Biol. Chem. 273*, 30448.
31. Wu, C.-F., and Chen, S.-H., (1988) *Biopolymers 27*, 1065.
32. Rosenzweig, A. C., Brandstetter, H., Whittington, D. A., Nordlund, P., Lippard, S. J., and Frederick, C. A. (1997) *Proteins: Struct., Funct., Genet. 29*, 141.
33. Jiang, Y., Wilkins, P. C., and Dalton, H. (1993) *Biochim. Biophys. Acta 1163*, 105.
34. Qian, H., Edlund, U., Powlowski, J., Shingler, V., and Sethson, I. (1997) *Biochemistry 36*, 495.
35. Krueger, J. K., Olah, G. A., Rokop, S. E., Zhi, G., Stull, J. T., and Trewhella, J. (1997) *Biochemistry 36*, 6017.
36. Krueger, J. K., Zhi, G., Stull, J. T., and Trewhella, J. (1998) *Biochemistry 37*, 13997.
37. Harpaz, Y., Gerstein, M., and Chothia, C. (1994) *Structure 2*, 641.

BI982991N